21, rue d'Artois, F-75008 PARIS
http : //www.cigre.org

CIGRE US National Committee
2023 Grid of the Future Symposium

Regional Inertia Estimation Using Ambient Synchrophasor Measurements

M. ELNASRY[1], L. ZHU[1]*, E. FARANTATOS[1], D. RAMASUBRAMANIAN[1], P. MITRA[1], V. SINGHVI[1], V. AJJARAPU[2]

[1]Electric Power Research Institute (EPRI), [2]Iowa State University
USA

SUMMARY

To overcome the drawbacks of the existing post-mortem inertia estimation approaches, this paper proposes an innovative algorithm for online ambient data-based regional inertia estimation. Inputs of the algorithm are the PMU measurements of tie line powers, locations of the machines inside the region of interest, available frequencies, and voltages, as well as the network admittance matrix. By utilizing voltage measurements, the algorithm estimates the load power response and subsequently determines the regional total import/export active power. Moreover, an aggregate acceleration power $\Delta\hat{P}$ is estimated using an aggregate governor model. The dynamic states of rotor speeds are derived from the available frequencies, and a regional equivalent rotor speed, denoted as $\hat{\omega}_{COI}$, is calculated. Estimated quantities are processed through a sliding window with controlled length, resulting in a sequence of inertia estimates. Each sliding window trains a transfer function model using system identification technique, which governs the relationship between $\Delta\hat{P}$ and $\hat{\omega}_{COI}$, to estimate a potential value for inertia. Various estimated values are validated and combined to obtain a final estimate. The algorithm performance has been evaluated using ambient data from the 2000-bus synthetic Texas grid model. The results demonstrate robust behaviour across different case studies.

KEYWORDS

Regional inertia estimation, ambient measurements, autoregressive moving average exogenous input (ARMAX), system identification, phasor measurement unit (PMU), rotor speed, voltage-dependent load.

lzhu@epri.com

1. Introduction

As utilities are transitioning towards a low-carbon future, there are increased concerns around system reliability, especially frequency security, which is a key component of reliable system operation. With the increasing penetration of inverter-based resources (IBRs) that continue to displace conventional synchronous machines, the overall system inertia is reduced, and this directly impacts the rate of change of frequency (ROCOF) that the power system is exposed to immediately following a disturbance. Higher ROCOF allows less time for frequency response services to act and hence threatens frequency load shedding (UFLS) or in more severe cases, system separation. Utilities worldwide have established planning procedures and operational constraints in the form of ROCOF constraints or critical inertia floors to accommodate existing equipment withstand and available reserve capabilities.

In this context, utilities monitor system inertia in their control rooms in real-time and look at forecasts. Estimating or measuring inertia accurately in real-time allows system operators to manage the grid and efficiently procure frequency response services. However, most of the control room inertia monitoring at this time is based on online EMS telemetered generating stations where the system inertia is the sum of the inertia of the machines that are synchronized at a specific time instant. Estimates from EMS-monitored generation do not account for the demand side inertia contribution from large industrial loads and demand side generation (e.g., embedded synchronous generation; combined heat and power plants that are not monitored in the EMS). In some cases, as in National Grid in Great Britain, this contribution has been found to be substantial, where the demand has been found to have an inertia constant of 1.832s [1]. Moreover, island systems like EirGrid in Ireland have registered high variability at daily and hourly demand side contribution to inertia [2].

In the context of the non-uniform expansion of IBRs, further concerns arise over regional inertia pockets, inertia centers separated by weak transmission lines. In such a scenario, the single-frequency models that many utilities still use for certain security assessments may no longer hold valid [1]. Considering these concerns, accurate real-time inertia estimation has gained significant interest in recent literature. Current industry practices and the latest inertia monitoring and estimation research have been summarized in [3]. Inertia estimation techniques can be broadly divided into large event-based techniques, which rely on large system events and can only be used for validation as postmortem [4], and wide area measurement-based techniques, which operate online based on ambient variations [5] or depend upon a modulated signal that is injected into the system [6]. In [7], event data is used for system inertia estimation, and the performance of inertia estimation for three different C37.118 compliant phasor measurement units (PMUs) are compared and found to be sufficient to support inertia estimation. In [8], system inertia is estimated based on outage scenarios using dynamic regressor extension and mixing. In [9], an autoregressive moving average exogenous input (ARMAX) model is used to estimate system inertia using PMU data and in [5], ARMAX models are used to estimate regional inertia. In [10], an alternative method that uses ambient data to estimate the regional concentration of inertia is presented. Furthermore, a continuous area-inertia measurement approach, capable of measuring area inertia and its implementation in the GB system, is discussed in [11].

This paper proposes a novel algorithm for application in real-time inertia estimation using ambient data. The method can be used for both system level and regional inertia estimation, where regional inertia refers to the cumulative contribution from a group of tightly coupled generators in a portion of the network that is weakly coupled to the rest of the system. The method is based on training a sequence of ARMAX models using estimated total import/export electrical power to/from the region, estimated governor response using an aggregate governor model, and calculated equivalent regional rotor speed from the available PMU frequencies. The proposed method requires notably fewer ARMAX models than [5] and the testing presented here indicates that it is far less sensitive to its parameterization than the method presented in [12]. Multiple case studies are performed to demonstrate the method effectiveness, and the proposed method is tested under different operating conditions.

This paper is structured as follows, Section II outlines the proposed algorithm and illustrates its different components, a case study is presented in Section III where results are discussed. Finally, Section VI concludes the paper.

2. Proposed Approach

This section illustrates how the proposed approach uses the available synchrophasor measurements to estimate the regional inertia. A general framework of the proposed approach is presented in Figure 1. The figure depicts the inputs to the algorithm, the estimated inertia as an output, and the processes embedded in between, including a load response estimator, governor response estimator, a rotor speed estimator, and an ARMAX model identification of the swing equation.

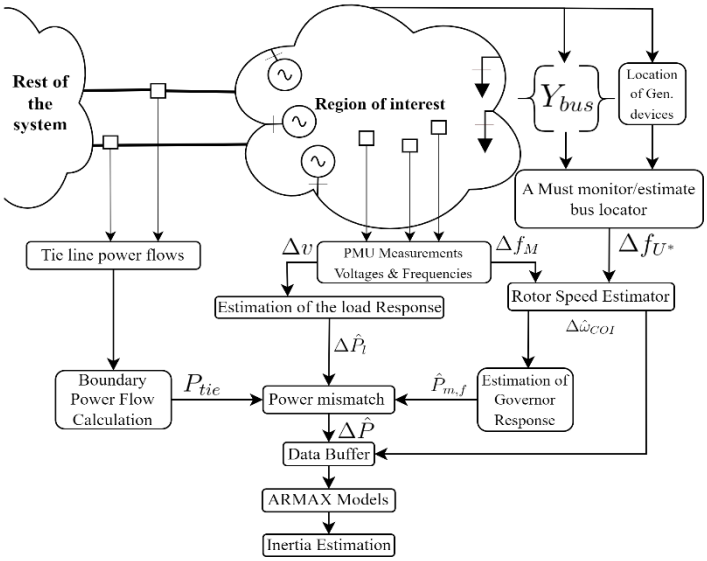

Figure 1. An overview of the proposed approach

2.1. Overview

The proposed method is an ambient data-based framework that can identify an equivalent swing equation for a sliding time window, as shown in Figure 2 and (1). An ARMAX system identification (ARMAX-SID) is used to define the underlying dynamics between the active power imbalance (ΔP) and the regional equivalent rotor speed (ω_{COI}).

Figure 2. Equivalent swing equation

$$2H\frac{d}{dt}\hat{\omega}_{COI} = \hat{P}_m(t) - P_{tie}(t) - \hat{P}_l(t) \quad (1)$$

where $P_m(t)$ denotes the mechanical power, $P_{tie}(t)$ denotes the tie line powers imported/exported to/from the region, and $P_l(t)$ denotes the region load power. $P_{tie}(t) + P_l(t)$ represents $P_e(t)$.

Unlike the tie line power, mechanical power cannot be measured, and the frequency responses to load noise/variations and distributed energy resources (DERs) uncertainties need to be estimated. This is done through a regional-level aggregate governor model where the estimation sensitivity to the model parameters is studied and the calculated $\Delta\hat{P}$ is exported to the ARMAX-SID. Moreover, the regional-level equivalent rotor speed (ω_{COI}) is calculated from a set of actual/virtual rotor speeds that need to be estimated.

The ambient data measured by PMU devices inside the region and on the tie-lines connecting it to the rest of the system are the inputs of the algorithm. Network data specifying a certain topology is also required for the estimation processes. The former is a limited set of the available frequency and voltage measurements in substations within the region of interest and a complete set of active power measurements from the boundary tie lines importing/exporting electrical power to/from it. While the latter includes the network admittance matrix, location of PMUs, location of the generation devices, an

approximate estimation of the aggregate load power in MVA inside the region, and aggregate governor model parameters, i.e., the installed capacity, an equivalent droop constant, and a dead-band if exists.

2.2. Estimation of equivalent regional rotor speed

For accurate inertia estimation, it is required to estimate the actual rotor speeds of the connected synchronous machines inside the study region or alternatively monitor/estimate the frequency at the point of interconnection of a non-synchronous device to its terminal bus and estimate its equivalent internal frequency (virtual rotor speed). Once the actual/virtual rotor speeds are estimated, an equivalent regional rotor speed $\widehat{\omega}_{COI}$ is calculated. This $\widehat{\omega}_{COI}$ is different from the COI frequency traditionally used in literature from the perspective that the traditional arithmetic mean of rotor speeds does not account for local frequency oscillations which are captured by our estimated equivalent $\widehat{\omega}_{COI}$. This guarantee capturing the frequency regulation from all connected generation devices or flexible loads and avoids the inertia estimation errors resulting from using frequencies instead of directly using frequencies for the estimation process. Since rotor speeds cannot be measured, a dynamic state estimation is implemented to get the rotor speeds from the network frequencies.

For this purpose, the algorithm implements a must-monitor/estimate bus locator to identify effective local points in the network where frequencies must be monitored with PMUs. However, since the measurement data is only a limited set of network frequencies, the algorithm implements a frequency divider formula (FDF), proposed by [13], to first estimate the required missing frequencies (if not already monitored by PMUs), and then estimate the actual/virtual rotor speeds of the connected synchronous/non-synchronous devices.

The must-monitor/estimate bus locator utilizes the connectivity of the network, i.e., the connectivity of generation devices to the network using the topology information represented by the admittance network Y_{bus} and the location of the generation devices. The required unmonitored frequencies along with the rotor speeds are estimated using the FDF which is discussed below.

The basic idea behind the FDF is considering the transmission system as a continuum [14] where the frequency changes at each point along the lines with some boundary conditions that must be satisfied. These frequency changes are governed by a divider formula like voltages and currents divider formulas. The boundary conditions that must be met by the frequency variation along the lines are the internal frequencies of the generation devices/DERs/flexible loads behind an equivalent transient reactance. The derivation from principles starts from how the current injections and bus voltages are linked through the admittance matrix of the network. This is the reason why the operator needs the knowledge of Y_{bus} at a certain topology and keep it updated after topology changes. However, the scope of this paper is the ambient data-based inertia estimation so the assumption of having Y_{bus} reasonable. The detailed analytical derivation can be found in [13] and [15], while here we directly implement the FDF with discussing in detail the modification we made for our application.

To clarify the concept, consider Figure 3 where a synchronous machine G_i is represented by an electro motive force (emf) with an internal frequency ω_{G_i} behind a transient reactance x'_{di} which connects it to a low voltage terminal bus BG_i. Note that the internal frequency (rotor speed ω_{G_i}) and, most probably, the low voltage terminal bus frequency f_{BG_i} are not monitored and must be estimated. Further, the low voltage terminal bus is connected to a monitored, as an assumption, high voltage bus with frequency $f_{BG_i}^{hv}$ which in turn is connected to monitored buses with frequencies f_{B_1}, f_{B_2}, …, f_{B_k}. In Figure 3, frequencies at blue coloured buses are assumed to be monitored while those of the black coloured buses are unmonitored and hence need to be estimated. The must-monitor/estimate bus locator determines the required buses using the admittance matrix which gives information about the connectivity of the generation device and its terminal buses.

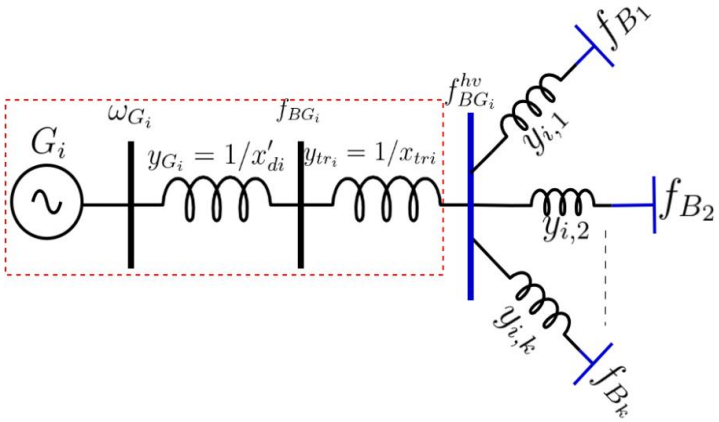

Figure 3. Clarification of the FDF concept with a general configuration

Assuming that $y_{BG_i}^{hv} = y_1 + y_2 + \cdots + y_k + y_{tr_i}$, i.e., the self-admittance of the high voltage terminal bus. It follows from the FDF that the high voltage bus frequency is approximated by (2) which gives an insight of how the method can determine the effective locations of PMUs to know the required local frequencies and estimate the frequencies which are not monitored.

$$y_{BG_i}^{hv} \times f_{BG_i}^{hv} = y_{tr_i} \times f_{BG_i} + y_1 \times f_{B_1} + y_2 \times f_{B_2} + \cdots + y_k \times f_{B_k} \tag{2}$$

where, $i = 1,2,\dots,n_g$ such that n_g is the number of connected devices which are required to get its contribution to the frequency regulation.

For the sake of generality, let $\boldsymbol{M}$ denote the limited set of network buses which are monitored, and the operator can observe their frequencies, voltages, and line powers. Let $\boldsymbol{U}$ denote the set of unmonitored buses, $\boldsymbol{U}^*$ is the set of unmonitored buses and selected by the must-monitor/estimate bus locator. Let the $\boldsymbol{B}$ denote the full set of network buses. The relationship between these sets can be mathematically expressed as follows.

$$\begin{aligned} \boldsymbol{B} &\coloneqq \boldsymbol{M} \cup \boldsymbol{U} \\ \boldsymbol{U}^* &\subseteq \boldsymbol{U} \end{aligned} \tag{3}$$

According to (3), the admittance matrix of the network is rearranged and written in (4).

$$Y_{bus} = \begin{pmatrix} Y_{MM} & Y_{MU} \\ Y_{UM} & Y_{UU} \end{pmatrix} \tag{4}$$

The dimension of the admittance matrix can be reduced according to the necessary local buses given by the must-monitor/estimate bus locator where the new reduced matrix Y_{bus}^{red} represents the study region as in (5).

$$Y_{bus}^{red} = \begin{pmatrix} Y_{MM} & Y_{MU^*} \\ Y_{U^*M} & Y_{U^*U^*} \end{pmatrix} \tag{5}$$

Note that the dimension of Y_{bus}^{red} is less than that of Y_{bus} since, for regional estimation, $\boldsymbol{U}^* \subset \boldsymbol{U}$. It follows that (2) can be generalized as given below in (6).

$$-Y_{MM} \times \boldsymbol{f_M} = Y_{MU^*} \times \boldsymbol{f_{U^*}} \tag{6}$$

and frequencies of the unmonitored set are approximated via (7).

$$\boldsymbol{f_{U^*}} = -Y_{MU^*}^{\dagger} \times Y_{MM} \times \boldsymbol{f_M} \tag{7}$$

where $\boldsymbol{f_M} = \begin{bmatrix} f_{m_1}(t) & f_{m_2}(t) & \cdots & f_{m_j}(t) \end{bmatrix}^\top$, and $\boldsymbol{f_{U^*}} = \begin{bmatrix} f_{u_1}(t) & f_{u_2}(t) & \cdots & f_{u_l}(t) \end{bmatrix}^\top$ are the frequencies of the j buses of the $\boldsymbol{M}$ set, and the l buses of the $\boldsymbol{U}^*$ set respectively and † is the matrix pseudo inverse. After estimating the necessary frequencies $\boldsymbol{f_{U^*}}$, the rotor speeds can be estimated each as an internal bus frequency behind the transient reactance. The setup for the rotor speed estimation is given below.

Let $\boldsymbol{h}$ denote a set of hypothetical buses different from those of the network. A hypothetical bus is a bus that is virtually located behind a transient reactance in case of the synchronous machine or behind an equivalent impedance that can be determined by the operator for each non-synchronous generating device depending on its capacity and dynamic behaviour [16]. The frequencies of the $\boldsymbol{h}$ set are the actual/ virtual rotor speeds. Following the same procedure, a new admittance matrix can be extracted now with further dimension reduction to represent the generation devices in the study region. Let Y_{bus}^{G} denote this generation admittance matrix which can be written in terms of the internal buses set $\boldsymbol{h}$ and the terminal buses set $\boldsymbol{T} = \{T_1, T_1^{hv}, T_2, T_2^{hv} \dots, T_{n_g}, T_{n_g}^{hv}\}$. Note that the terminal buses T_i, T_i^{hv} for the i^{th} generation device are B_{G_i} and $B_{G_i}^{hv}$ as depicted in Figure 3. In practice, $B_{G_i}^{hv} \in \boldsymbol{M}$ (monitored) while $B_{G_i} \in \boldsymbol{U}^*$ (unmonitored but estimated with (7)) and $\boldsymbol{T} \subseteq \boldsymbol{U}^*$. The Y_{bus}^{G} is given as follows.

$$Y_{bus}^{G} = \begin{pmatrix} Y'_{TT} & Y_{Th} \\ Y_{hT} & Y_{hh} \end{pmatrix} \tag{8}$$

In (8), Y'_{TT} is calculated by modifying Y_{TT} with the internal equivalent impedances such that:

$$Y'_{TT} = Y_{TT} + Y_G \tag{9}$$

Y_G is a diagonal matrix with the same dimension as Y_{TT} and its main diagonal entry is $1/x'_d$ if the generating device is installed on the corresponding bus and zero otherwise. $Y_{Th}(T_i, h_i)$ has a nonzero entry equal to $1/x'_{di}$ if the i^{th} generation device (with internal bus h_i) is connected to the terminal bus T_i. Y_{hh} is a square diagonal matrix where the entry corresponding to the i^{th} generation device equals $-1/x'_{di}$. Finally, $Y_{hT} = Y_{Th}^{\top}$. The rotor speeds can be estimated as given by (10).

$$\widehat{\boldsymbol{\omega}}_{\boldsymbol{G}} = -Y_{Th}^{\dagger} Y'_{TT} \times \boldsymbol{f}_{\boldsymbol{T}} \tag{10}$$

The regional equivalent rotor speed $\widehat{\omega}_{COI}$ is calculated as the arithmetic mean of the estimated rotor speeds. If the region has n_{syn} large synchronous machines with known inertia constants $H_1, H_2, \dots H_{n_{syn}}$ to the operator, the calculation of the $\widehat{\omega}_{COI}$ can be improved using (11).

$$\widehat{\omega}_{COI} = avg\left\{\left(\frac{1}{\sum_{n=1}^{n_{syn}} H_n} \sum_{n=1}^{n_{syn}} \omega_{G_n} \times H_n\right), \left(\frac{1}{n_g - n_{syn}} \sum_{n=n_{syn}+1}^{n_g} \omega_{G_n}\right)\right\} \tag{11}$$

Once the proposed equivalent rotor speed frequency is estimated, it can be exported to the governor and load models which are discussed in the next subsection.

2.3. Estimation of active power mismatch

The main task in this subsection is to estimate the time series of the active power mismatch for each time window, i.e., $\Delta\hat{P}^i(t)$. This is mathematically assumed to be as follows.

$$\Delta\hat{P}^i(t) = \hat{P}_m^i(t) - P_e^i(t) \tag{12}$$

An aggregate governor estimates the active power imbalance in the region based on the boundary power flow and equivalent frequency $\widehat{\omega}_{COI}$, as summarized in Figure 4. The dashed boxes denote data vectors of the i^{th} time window. The time frame of each sliding time window includes the pre-analysis time T_{pre}, the post analysis time T_{post}, and the gap duration T_{gap} between them if exists. Accordingly, the i^{th} sliding window for active power in Figure 4 is separated into two blocks ($T_{gap} = 0$): $P_{tie,pre}^i$, and $P_{tie,post}^i$, and the same is true for the frequency, $\widehat{\omega}_{COI,pre}^i$, $\widehat{\omega}_{COI,post}^i$ and the average of voltage variations in a limited set of high voltage buses v_{pre}^i, and v_{post}^i. An estimation time T_{est} is defined by the user to govern the moving length of the sliding window. In other words, the pre, gap, and post analysis of the data is repeated after nT_{est} where $n = 0,1, \dots$, and so on.

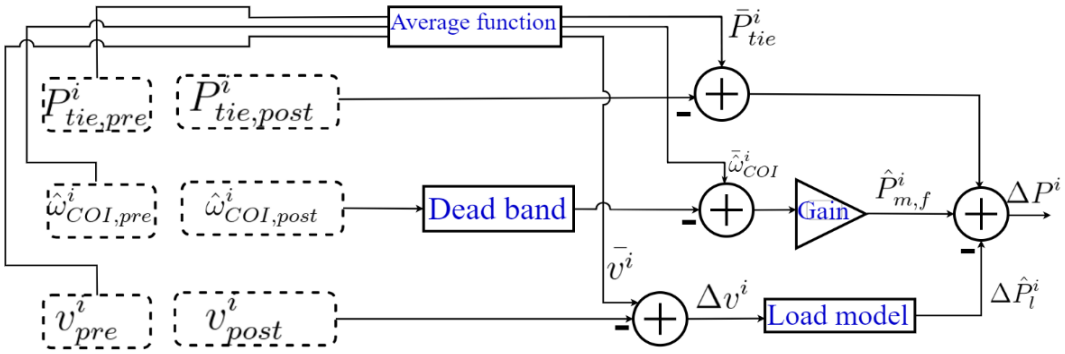

Figure 4. Block Diagram of the power mismatch estimation

It is assumed that the region is balanced with mechanical power equal to $\bar{P}^i_{tie} + P_{l0}$ during the pre-time analysis of each time window i. Such that $\bar{P}^i_{tie}$ is the average of the tie line power during T_{pre} of the i^{th} time window while P_{l0} is an aggregated load power which is a constant MW for the study region and could be known to the operator.

Any following change in mechanical power is determined by the frequency change in the region during T_{post} period and denoted as $\hat{P}^i_{m,f}$ to represent the frequency sensitive component of P^i_m. A delay in the realistic governor response can be represented. The average of $\hat{\omega}^i_{COI,pre}$ is used to correct $\hat{\omega}^i_{COI,post}$ for the frequency deviation during the T_{pre} (e.g. if the average of $\hat{\omega}^i_{COI,pre}$ is 59.95 Hz and the frequency in the first sample of $\hat{\omega}^i_{COI,post}$ is 59.94 Hz then $\Delta\hat{\omega}^i_{COI}$ considered by the imbalance estimation for the first sample will be 0.01 Hz). This is necessary to avoid double counting of the governor response for this pre-existing deviation (once in $\bar{P}^i_{tie}$ and again in $\hat{P}^i_{m,f}$) due to the assumption that the system is balanced at the start of the post-time window. Note, this process is resilient in the presence of frequency control response FCR provided by non-synchronous resources, e.g., battery energy storage, as they will directly impact the measured electrical power.

Furthermore, the aggregate governor parameters of dead-band and gain need not be highly accurate and can be based on the standard grid code requirements. On the other hand, the electrical power for a specific time window, see Figure 4, is represented by the tie line power $P^i_{tie,post}$, and the changes in the load power ΔP^i_l during T_{post}. Mechanical and electrical power of each time window expressed as:

$$\hat{P}^i_m(t) = \bar{P}^i_{tie}(t) + P_{l0} + \hat{P}^i_{m,f}(t) \tag{13}$$

$$\hat{P}^i_e(t) = P^i_{tie,post}(t) + \Delta\hat{P}^i_l(t) \tag{14}$$

The load response $\Delta\hat{P}^i_l$ is estimated using the PMU voltage measurements which is used along with an approximated ZIP load model, for simplicity in this study, to account for variations of the load power during different time windows. Given load model parameters, the constant power coefficient P_p, the constant current parameter P_I, and the constant admittance load P_Z, $\Delta\hat{P}^i_l(t)$ is mathematically described for a specific i^{th} time window as:

$$\Delta\hat{P}^i_l(t) = P_{l0} \times \left[P_p + P_I \times \Delta v^i + P_Z \times \Delta {v^i}^2\right] \tag{15}$$

Δv^i is the voltage variations for the i^{th} time window, i.e., the difference between v^i_{post} and $\bar{v}^i$.

2.4. ARMAX system identification and inertia estimation candidates

The developed method uses an ARMAX-SID for the purpose of identifying the dynamics between the $\hat{\omega}_{COI}$, and $\Delta\hat{P}$. ARMAX, i.e., Autoregressive Moving Average with Exogenous inputs is a type of time-series model used for prediction and forecasting. It is an extension of the ARMA (Autoregressive Moving Average) model that incorporates additional exogenous (external) variables that may influence the time series being analysed. ARMAX models are characterized by the order of the autoregressive

component, the order of the moving average component, and the number of exogeneous variables. The ARMAX model can be expressed mathematically as follows:

$$\begin{aligned} \mathrm{y(t)} = \theta_1 y(t-1) + \theta_2 y(t-2) + \cdots + \theta_p y(t-p) + \beta_1 x_1(t) + \beta_2 x_2(t) \\ + \cdots + \beta_r x_r(t) + \epsilon(t) + \varphi_1 \epsilon(t-1) + \varphi_2 \epsilon(t-2) + \cdots \\ + \varphi_q \epsilon(t-q) \end{aligned} \tag{16}$$

where: $y(t)$ represents the time series being modelled, $x_i(t)$ represents the exogenous variable i at time t, θ's are the autoregressive coefficients, β's are the coefficients for the exogenous variables, $\epsilon(t)$ represents the white noise error term, and φ's are the moving average coefficients for the error term.

ARMAX is preferred over other methods, e.g., AR (Auto-Regressive), ARX (autoregressive with exogenous terms), ARMA (autoregressive moving average) since ARMAX is the most comprehensive model amongst these options [5], [9]. Its output is characterized as the sum of three regression terms containing past input, output, and disturbances, whereas the other methods only comprise two of the three terms. The exogeneous variables gives the ARMAX the advantage to represent uncertainties in the power system such as load changes, and renewable energy.

Data ($\widehat{\omega}_{COI}$, and $\Delta\hat{P}$) are inputted for the ARMAX-SID and ARMAX models (equal to the number of user-defined sliding time windows) are trained. ARMAX models are trained with $\Delta\hat{P}$ as an exogeneous input and $\widehat{\omega}_{COI}$ as an output. A polynomial model is identified for each time window and coefficients in (16) are calculated. The i^{th} identified ARMAX model is used to get the frequency response ω^i_{step} of a unit step change in ΔP^i and ROCOF is calculated for each time window as $\frac{d}{dt}\omega^i_{step}$. The traditional swing equation, see Figure 2, is used for the ROCOF calculation and hence the inertia estimation. Although this is the traditional form of the swing equation, it is used in this context with the estimated signals of $\widehat{\omega}_{COI}$, and $\Delta\hat{P}$ which makes the inertia estimated is the effective inertia that relates the local frequency deviations with the power mismatch. The estimation candidate for each time window could be calculated using the initial value theorem as given in (17).

$$H^i_{est} = 0.5 \frac{1}{\frac{d}{dt}\omega^i_{step}|_{t=0}} \tag{17}$$

Alternatively, a second order curve fitting could be implemented for the generated model outputs $\frac{d}{dt}\omega^i_{step}(t)$ where the initial value of the fitted parabola is considered the candidate estimate. This can reject the imperfect models that produce poor estimates.

2.5. Data buffer and sliding windows

The methodology is based on the serial processing of a data buffer (with length of b seconds) that is refreshed every r seconds. The method processes each buffer and then based on this, updates the regional inertia estimate every r seconds. The data buffer is broken up into N sliding windows of frequency, voltage, and active power data, each of which is used to calculate a candidate inertia estimate. The set of N candidate values are blended to create a final estimate of inertia that represents the result for this data buffer. Here the blending process simply entails taking the mean of the estimates after discarding those estimates below the 5th percentile and above the 95th percentile of the estimate range.

3. Case study on synthetic Texas grid model

The performance of the developed method is tested via different test cases and operating scenarios. We limit our presentation to a relatively large and practical Texas test system. Simulations are conducted using the commercial software PSS/E which can efficiently perform dynamic simulations of large-scale power systems.

3.1. Study system

The 2000-bus synthetic Texas grid model has been built from publicly available information by Texas A&M University [17]. The system has 544 generating devices (among which 87 renewables), and 1350

Figure 5. Synthetic Texas grid model: A map of the electrical regions

loads. As shown in Figure 5, the system is divided into 8 areas. The South area is selected as the study region, in which there are 41 in-service synchronous generators with 7,448 MVA in capacity. Each synchronous generator has a governor model without dead-band, and the droop is 4% or 5%. There are 11 renewable generators with totally 2,512 MVA in capacity in the South area. Each renewable generator is modelled by the WECC generic converter model and electric control model. No inertia contribution from these renewable generators. The total load in the South area is 6,751 MW. Also, there are 25 tie-lines between the study region (South) and its neighbour regions (West, South Central, and Coast). The ground truth total rotating inertia of the southern region is 34,610 MVAs. A load in Coast area is modulated to mimic $250\ s$ long ambient data measurements. The PMU reporting rate is 30 Hz.

3.2. Inertia estimation results

Machines low voltage terminal buses are unmonitored, and their frequencies need to be estimated through the FDF. The FDF is again used to estimate rotor speeds from the set of observed/estimated frequencies, and finally their arithmetic mean $\hat{\omega}_{COI}$ is calculated. Figure 6 shows $\hat{\omega}_{COI}$ versus the average of the available frequencies. Although the difference between them, with ambient data, is not significant, the inertia estimation is impacted when using the frequency instead of $\hat{\omega}_{COI}$. The estimated governor response, and the frequency variations of the 1st time window ($T_{pre} = 10\ s, T_{post} = 30\ s, \& T_{gap} = 0$) are depicted in Figure 7. This is obtained with a linear governor model with droop constant of 5%, zero dead-band, and installed capacity of 7500 MW. Voltages are used to estimate the aggregate load variations of the study region with an assumed static load model of 20% constant power load, 30% constant admittance load, and 50% constant current load. The estimated load response $\widehat{P}_l$ for the 1st window is shown in Figure 8. The estimated $\hat{\omega}_{COI}$ and $\Delta\widehat{P}$ are inputted to the ARMAX-SID and the inertia estimates are depicted in Figure 9.

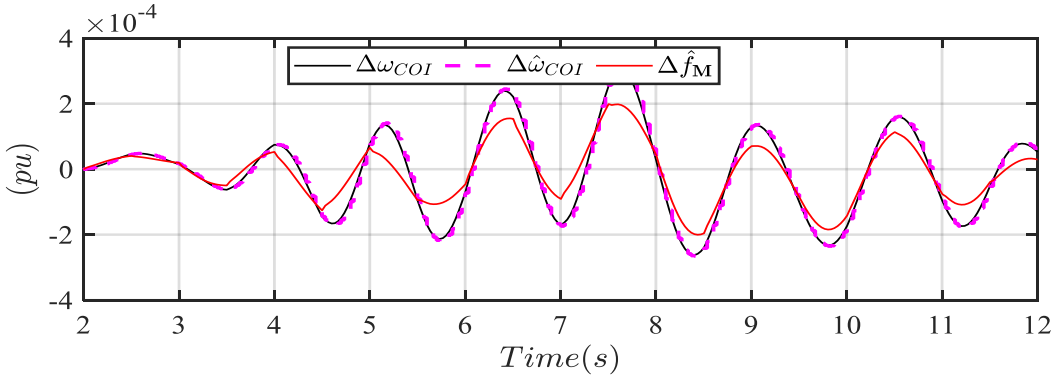

Figure 6. Actual/estimated equivalent rotor speed versus the average of monitored frequencies.

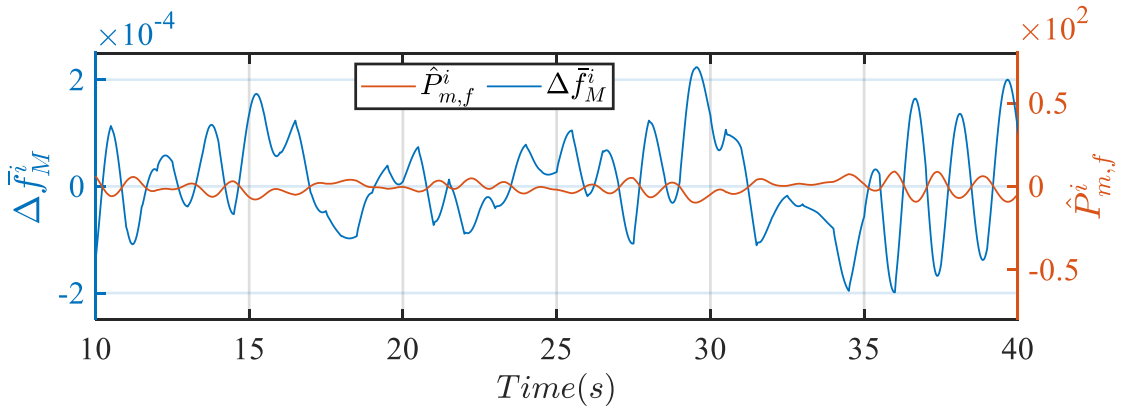

Figure 7. Estimation of the governor response versus the frequency variations

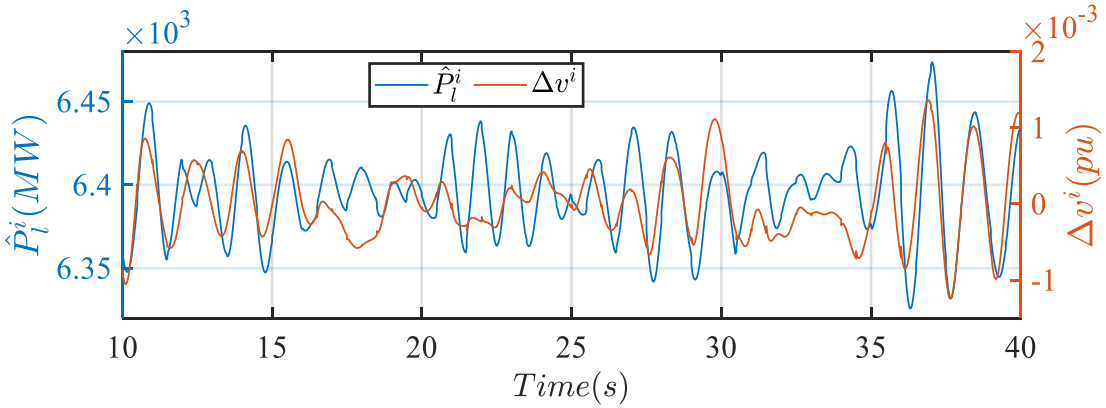

Figure 8. Estimation of the load response versus the voltage variations

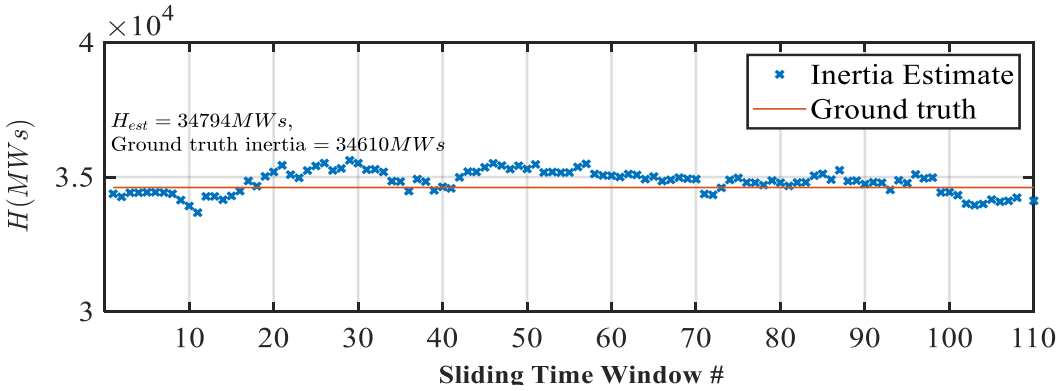

Figure 9. Inertia estimation for sliding time windows

The inertia estimation results with different scenarios are given in Table 1. The addressed scenarios depict the performance of the proposed method with the governor response estimation, the load response estimation, the estimated rotor speed, and finally the impact of those on the estimated inertia. Using only tie-line powers and ignoring the load response, which is approximated here by its voltage dependency, impacts the results and causes underestimating the inertia, see Scenario #4. On the other hand, direct use of frequencies of the network without approximating the internal rotor speeds causes an overestimation of the inertia (Scenario #3). The governor model with its parameters, i.e., dead-band, droop constant, installed MW capacity contributes in accurately estimating the power imbalance.

Table 1. Inertia estimation results

Scenario NO.	Governor response estimation	Voltage-dependent load estimation	Rotor speed estimation	$\widehat{\boldsymbol{H}}$ $(\boldsymbol{MWs})$	Error (%)
1	Deactivated	Deactivated	Deactivated	76,579	121.0
2	Activated	Deactivated	Deactivated	70,264	103.0
3	Activated	Activated	Deactivated	41,624	26.0
4	Activated	Deactivated	Activated	29,765	-14.0
5	Activated	Activated	Activated	34,794	0.5

4. Conclusion

In conclusion, this paper proposes a novel algorithm designed to estimate regional inertia in real-time using ambient data. By combining ARMAX based system identification, an efficient governor approximation, an aggregate load model that adapts to ambient changes, and a dynamic state estimator capable of estimating internal frequencies and rotor speeds, the proposed method offers continuous and accurate estimations without the need for specific events. The application of this methodology on the Texas grid model 2000 bus system demonstrates its excellent performance. Furthermore, the study investigates the impact of each component by deactivating/activating them and assessing their influence on estimation accuracy. The results highlight the significance of the aggregate load models in estimating load response and emphasize the efficacy of the rotor speed estimator in effectively approximating the virtual regional equivalent rotor speed. Overall, the proposed method represents a valuable contribution to the field of inertia estimation, offering a simple parameterization and a robust solution for real-time estimation of regional inertia using ambient data.

BIBLIOGRAPHY

[1] MIGRATE Project, "D2.3: Lessons Learned from Monitoring & Forecasting KPIs on Impact of PE penetration," 2018. [Online]. Available: https://www.h2020-migrate.eu/downloads.html.

[2] M. R. Bank, Tavakoli, M. Power, L. Ruttledge, and D. Flynn, "Load inertia estimation using white and grey-box estimators for power systems with high wind penetration," *Power Plants and Power Systems Control*, 2012.

[3] EPRI, "Online Inertia Estimation & Monitoring: Industry Practices & Research Activities," Power Delivery & Utilization, EPRI, Knoxville, 2019.

[4] P. Wall and V. Terzija, "Simultaneous Estimation of the Time of Disturbance and Inertia in Power Systems," *IEEE Transactions on Power Delivery*, vol. 29, no. 4, pp. 2018-2031, Aug. 2014.

[5] K. Tuttelberg, J. Kilter, D. Wilson and K. Uhlen, "Estimation of Power System Inertia From Ambient Wide Area Measurements," *IEEE Trans. Power Systems*, vol. 33, no. 6, p. 7249–7257, 2018.

[6] B. Berry, "Inertia Estimation Methodologies vs Measurement Methodology: Impact on System Operations," in *CIGRE*, Aalborg Symposium, Denmark, June 2019.

[7] P. Wall, P. Regulski, Z. Rusidovic and V. Terzija, "Inertia estimation using PMUs in a laboratory," in *IEEE PES Innovative Smart Grid Technologies*, Istanbul, 2014.

[8] J. Schiffer, P. Aristidou and R. Ortega, "Online Estimation of Power System Inertia Using Dynamic Regressor Extension and Mixing," *IEEE Trans. Power Systems*, vol. 34, no. 6, p. 4993–5001, 2019.

[9] L. Lugnani, D. Dotta, C. Lackner and J. Chow, "ARMAX-based method for inertial constant estimation of generation units using synchrophasors," *Electr. Power Syst. Res.*, vol. 180, 2020.

[10] F. Zeng, J. Zhang, Y. Zhou and S. Qu, "Online Identification of Inertia Distribution in Normal Operating Power System," *IEEE Trans. Power Systems*, vol. 35, no. 4, p. 3301-3304, 2020.

[11] D. H. Wilson, S. Norris, N. Al-Ashwal, P. McNabb, P. Ashton and J. Yu, "Stability challenges and solutions for reducing inertia: PMU-based measurement and machine-learning forecasting," in *CIGRE Paris Session*, Paris, 2020.

[12] M. Liu, J. Chen and F. Milano, "On-Line Inertia Estimation for Synchronous and Non-Synchronous Devices," *IEEE Transactions on Power Systems*, vol. 36, no. 3, pp. 2693-2701, 2021.

[13] F. Milano, and A. Ortega, " Frequency divider", *IEEE Transactions on Power Systems*, vol. 32, no. 2, pp. 1493-1501, 2016.

[14] A. Semlyen, "Analysis of Disturbance Propagation in Power Systems Based on a Homogeneoue Dynamic Model," *IEEE Transactions on Power Apparatus and Systems*, vol. PAS-93, no. 2, pp. 676-684, 1974.

[15] F. Milano, A. Ortega, "A method for evaluating frequency regulation in an electrical grid-Part I: Theory", *IEEE Transactions on Power Systems*, vol. 36, no. 1, pp. 183-193, 2020.

[16] F. Milano, A. Ortega, "A method for evaluating frequency regulation in an electrical grid-Part II: Applications", *IEEE Transactions on Power Systems*, vol. 36, no. 1, pp. 194-203, 2020.

[17] A. B. Birchfield; T. Xu; K. M. Gegner; K. S. Shetye; T. J. Overbye, "Grid Structural Characteristics as Validation Criteria for Synthetic Networks", *IEEE Transactions on Power Systems*, vol. 32, no. 4, pp. 3258-3265, 2017.